



# Evidence of disrupted rhombic lip development in the pathogenesis of Dandy–Walker malformation

Parthiv Haldipur<sup>1</sup> · Silvia Bernardo<sup>2</sup> · Kimberly A. Aldinger<sup>1,3</sup> · Tarika Sivakumar<sup>1</sup> · Jake Millman<sup>1</sup> · Alexandria H. Sjoboen<sup>1</sup> · Derek Dang<sup>1</sup> · Danilo Dubocanin<sup>1</sup> · Mei Deng<sup>4</sup> · Andrew E. Timms<sup>5</sup> · Brian D. Davis<sup>6</sup> · Jasmine T. Plummer<sup>6</sup> · Kshitij Mankad<sup>7</sup> · Ozgur Oztekin<sup>8</sup> · Lucia Mangano<sup>9</sup> · Fabien Guimiot<sup>10</sup> · Homa Adle-Biassette<sup>11,12</sup> · Rosa Russo<sup>13</sup> · Joseph R. Siebert<sup>14</sup> · Debora Kidron<sup>15</sup> · Giulia Petrilli<sup>16</sup> · Nathalie Roux<sup>16</sup> · Ferechte Razavi<sup>16</sup> · Ian A. Glass<sup>1,3,4</sup> · Cira Di Gioia<sup>9</sup> · Evelina Silvestri<sup>17</sup> · Kathleen J. Millen<sup>1,3,4</sup>

Received: 1 April 2021 / Revised: 26 June 2021 / Accepted: 24 July 2021 / Published online: 4 August 2021  
© The Author(s), under exclusive licence to Springer-Verlag GmbH Germany, part of Springer Nature 2021

## Abstract

Dandy–Walker malformation (DWM) and Cerebellar vermis hypoplasia (CVH) are commonly recognized human cerebellar malformations diagnosed following ultrasound and antenatal or postnatal MRI. Specific radiological criteria are used to distinguish them, yet little is known about their differential developmental disease mechanisms. We acquired prenatal cases diagnosed as DWM and CVH and studied cerebellar morphobiometry followed by histological and immunohistochemical analyses. This was supplemented by laser capture microdissection and RNA-sequencing of the cerebellar rhombic lip, a transient progenitor zone, to assess the altered transcriptome of DWM vs control samples. Our radiological findings confirm that the cases studied fall within the accepted biometric range of DWM. Our histopathological analysis points to reduced foliation and inferior vermian hypoplasia as common features in all examined DWM cases. We also find that the rhombic lip, a dorsal stem cell zone that drives the growth and maintenance of the posterior vermis is specifically disrupted in DWM, with reduced proliferation and self-renewal of the progenitor pool, and altered vasculature, all confirmed by transcriptomics analysis. We propose a unified model for the developmental pathogenesis of DWM. We hypothesize that rhombic lip development is disrupted through either aberrant vascularization and/or direct insult which causes reduced proliferation and failed expansion of the rhombic lip progenitor pool leading to disproportionate hypoplasia and dysplasia of the inferior vermis. Timing of insult to the developing rhombic lip (before or after 14 PCW) dictates the extent of hypoplasia and distinguishes DWM from CVH.

**Keywords** Dandy–Walker malformation · Cerebellum · Cerebellar vermis hypoplasia · Rhombic lip · Development

## Introduction

Human cerebellar malformations are diverse and commonly recognized birth defects, frequently associated with significant developmental disabilities [1]. Dandy–Walker malformation (DWM) is one of the most well-known cerebellar

malformations, first recognized and defined by autopsy studies from the late 1860s to 1950s [7, 12, 32]. DWM is now diagnosed by brain imaging studies (Fig. 1a, b, d–f) and strictly defined by cerebellar hypoplasia predominantly affecting the posterior vermis, upward rotation of the cerebellum away from the brain stem causing elevation of the tentorium (Fig. 1b, white arrowhead), and a dilated fourth ventricle (Fig. 1b, c, asterisk) within an enlarged posterior fossa (Fig. 1b, red arrowhead) [5, 6, 8]. DWM can occur in isolation or as part of syndrome including other congenital defects [1, 2].

While there is a consensus regarding the distinctive postnatal brain imaging features of true DWM, the developmental origins of these features remain unclear and prenatal diagnosis has historically been difficult with poor correlation

---

Silvia Bernardo, Kimberly A. Aldinger, Tarika Sivakumar and Jake Millman have contributed equally to this work.

✉ Parthiv Haldipur  
parthiv.haldipur@seattlechildrens.org

✉ Kathleen J. Millen  
kathleen.millen@seattlechildrens.org

Extended author information available on the last page of the article

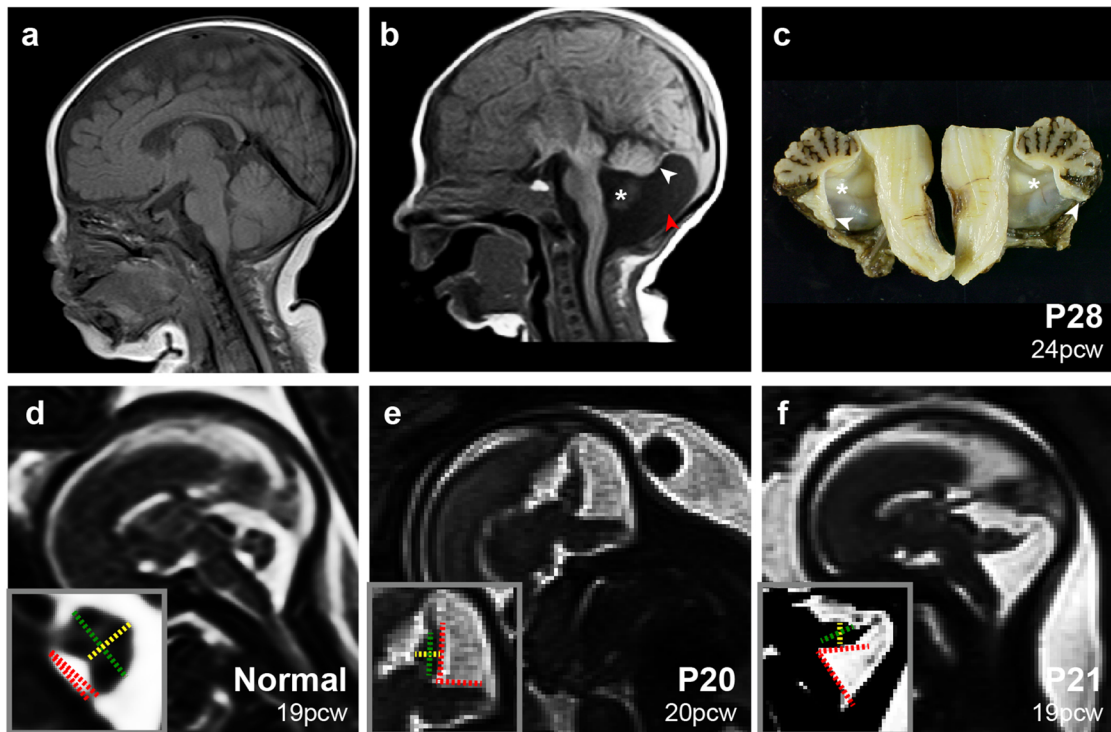


Table 1	Vermian APD (mm)	Vermian CCD (mm)	PCA (mm)
Normal Mean	7.08 (SEM 0.611) (20-24 GW n=169)	10.13 (SEM 0.644) (20-24 GW n=169)	9.1 (SEM 0.611) (Range 20-24 GW n=80)
Dandy Walker Mean	4.56 (SEM 0.217) (20-22 GW n=8)	6.56 (SEM 0.217) (20-22 GW n=8)	65.75 (SEM 5.48) (20-22 GW n=8)
18pcw Normal	5.5 - 6.3 - 7.2 (n=23; 5 - 50 - 95 <sup>th</sup> percentile)	7.7 - 9.0 - 10.0 (n=23; 5 - 50 - 95 <sup>th</sup> percentile)	4-17 (Range: 20-24 GW; n=80)
18(+3)pcw DWM (P15)	4	6	54
19pcw Normal	6.0 - 6.7 - 7.8 (n=73; 5 - 50 - 95 <sup>th</sup> percentile)	8.3 - 9.8 - 10.9 (n=73; 5 - 50 - 95 <sup>th</sup> percentile)	4-17 (Range: 20-24 GW; n=80)
19pcw DWM (P21)	4.5	6.5	68
19pcw DWM (P22)	5	7	71
19(+3)pcw DWM (P18)	4	6	55
19(+3)pcw DWM (P17)	4	6	50
20pcw Normal	6.4 - 7.3 - 8.4 (n=43; 5 - 50 - 95 <sup>th</sup> percentile)	8.9 - 10.6 - 11.9 (n=43; 5 - 50 - 95 <sup>th</sup> percentile)	4-17 (Range: 20-24 GW; n=80)
20(+1)pcw DWM (P20)	5	7	80
21pcw Normal	6.8 - 7.8 - 9.0 (n=22; 5 - 50 - 95 <sup>th</sup> percentile)	9.5 - 11.4 - 12.8 (n=22; 5 - 50 - 95 <sup>th</sup> percentile)	4-17 (Range: 20-24 GW; n=80)
22pcw Normal	7.2 - 8.3 - 9.6 (n=22; 5 - 50 - 95 <sup>th</sup> percentile)	7.2 - 8.3 - 9.6 (n=22; 5 - 50 - 95 <sup>th</sup> percentile)	4-17 (R20-24 GW; n=80)

**Note:** SEM indicates standard error of mean; APD: Antero-posterior diameter (green); CCD: Cranio-caudal diameter (yellow); PCA: Ponto-cerebellar angle (red); GW: age in gestational weeks; mm: millimeter. Normal values of APD, CCD and PCA listed are from *Conte et al., 2018* and *Volpe et al., 2012*.

**Fig. 1** Cerebellar morphobiometry in Dandy–Walker malformation (DWM). Postnatal MRI through midsagittal plane in normal (a) and DWM (b), with the ‘tail sign’ indicated (white arrowhead). DWM is characterized by cerebellar vermis hypoplasia, a dilated 4th ventricle (white asterisk) and an enlarged posterior fossa (red arrowhead). Midsagittal section of a 24pcw DWM hindbrain shows characteristic ‘tail sign’ (white arrowhead) and hypoplasia of the vermis (c). Fetal MRI in normal (d) and DWM (e, f), where tegmento-vermian angle (red), cranio-caudal diameter (green) and antero-posterior diameter (yellow) are measured and shown as dashed lines. Measurements for APD, CCD, and TVA in five normal cases (table, grey) and six DWM cases (table, orange) are compared. Data is represented in percentiles and mean  $\pm$  standard error of mean

between prenatal imaging and postnatal outcome [9, 10, 27, 28, 31]. Recently, imaging studies have suggested that a “tail sign”, an aberrant posterior vermis lobule extending into an enlarged fourth ventricle, represents a diagnostic feature of prenatal DWM and distinguishes DWM from other cerebellar malformations (Fig. 1b, c, white arrowhead) [8]. Since there is limited literature on the prenatal or postnatal pathology of human DWM [13, 22, 30], the origin of this tail and its relationship to postnatal DWM pathology remain unclear.

We previously found that *FOXC1* and *ZIC1/4* deletions are causative for a small subset of syndromic DWM cases [2, 16]. Our mouse modeling studies of *Foxc1* function pointed to the cerebellar rhombic lip as a focus for DWM pathology [20, 21]. The rhombic lip is a transient progenitor zone during mouse cerebellar development that gives rise to a subset of cerebellar nuclei, unipolar brush cells, and cerebellar granule neuronal progenitors (GNP) which then give rise to granule neurons, the predominant neuronal cell type of the postnatal cerebellum [23]. Hypomorphic mesenchymal to cerebellar signaling in mice decreases production of posterior vermis fated cerebellar GNPs and also causes abnormal production and migration of unipolar brush cells. This results in posterior-predominant vermis hypoplasia with an unpaired posterior folium often observed in postnatal DWM cases. Furthermore, there are striking similarities between the developing cerebella of *Foxc1* mouse mutants and rare human fetal samples with heterozygous *FOXC1* deletions [20, 21]. Although mouse models of DWM have implicated the rhombic lip as a focus of DWM developmental pathology, we recently described dramatic spatiotemporally expanded progenitor zones in human vis-à-vis mice, including the rhombic lip [18]. Thus, comparisons across species are limited. Furthermore, our mouse models do not readily explain the mechanisms of DWM, although recent genetic analyses indicate that aberrant cerebellar vasculature development may be a contributing factor [4].

To investigate the developmental mechanisms of human DWM pathology, we acquired the first ever large cohort of fetal samples diagnosed with DWM or cerebellar vermis hypoplasia (CVH) based on radiological criteria, confirmed by autopsy and pathology. Almost all were without genetic

diagnosis. We sought to identify common features linking all of the DWM cases and define the developmental features distinguishing DWM from other variants of cerebellar hypoplasia. Through morphological, immunohistochemical and transcriptomic analyses, we also defined the nature of the DWM tail. Our comprehensive analyses using multiple approaches defines mechanisms of disease at the cellular and molecular level. We propose a unified developmental model for DWM and CVH, defining significant differences in developmental timing of the primary insults for these important cerebellar malformations.

## Materials and methods

### Human tissue collection

A total of 54 pathological specimens (26 DWM, 5 CVH cases and 23 age-matched normal controls) have been described in the study (Suppl. Table S1, online resource). All human material was obtained in accordance with approved IRB protocols at Seattle Children’s Research Institute. Normal tissue samples were collected by the Human Developmental Biology Resource (HDBR), located at University College London, and Newcastle University, United Kingdom and the Brain Defects Birth Laboratory (BDRL) at the University of Washington, Seattle, WA, while mid and late gestation tissue was collected at Hôpital Necker–Enfants Malades in Paris, France. Samples were collected following appropriate consent and in strict accordance with institutional and legal ethical guidelines. DWM and CVH samples were obtained from archival collections in United States, Italy, France and Israel. Complete autopsies were performed on all DW and CVH cases using standardized protocols. Tissue was fixed in formalin (pH 7.6) and embedded in paraffin. Sagittal sections of 4–5  $\mu$ m thickness were cut using a microtome (Leica RM 2135) and placed on Superfrost Plus white slides (VWR international, USA). Slides were stored at room temperature until immunostaining was performed. Some of the cases used in this study have been described previously [13, 18, 20].

### Fetal and postnatal imaging

Standard MR imaging sequences evaluated in the assessment of the brain morphology. The key sequence was Sagittal T1/T2 images. Sagittal midline T2 slices were used for biometric measurements with red representing the tegmento-vermian which is the angle formed by the intersection of two lines, the first line along the dorsal surface of the brainstem and the second along the ventral surface of the vermis. Normally the angle is close to 0° and the increase of the measure is often associated with posterior fossa malformations (for

DWM > 45°). Also measured were the cranio-caudal vermian diameter (in green) and the antero-posterior vermian diameter (in yellow).

## Histology

Cerebellar tissue was fixed in formalin or 4% PFA and then processed through graded alcohols and changes of xylene and subsequently embedded in paraffin wax prior to sectioning. Sections were collected at 4 µm. Cresyl violet, and Hematoxylin and Eosin (H&E) staining were carried out as previously described [19].

## Immunohistochemistry

Immunohistochemistry was performed as previously described [18]. Briefly, sections were deparaffinized in Xylene, rehydrated in alcohol gradients and subjected to heat mediated antigen retrieval followed by blocking and permeabilization with 5% normal goat serum (Vector laboratories, S-1000) containing 0.35% triton X. Primary antibodies were incubated overnight at 4 °C. The following primary antibodies were used: KI67 (DAKO, M7240, mouse, 1:50), SOX2 (Thermofisher, PA1-094, Rabbit, 1:200), β-III Tubulin (Promega, G712A, Mouse, 1:1000), Calbindin (Swant, CD38, rabbit, 1:3000), PAX6 (Biolegend, 901301, rabbit, 1:300), TBR2 (Thermofisher, 14-4875-82, mouse, 1:250), GFAP (DAKO, Z0034, rabbit, 1:1000), CD34 (DAKO, M716501-2, Mouse, 1:100) and phospho-vimentin (MBL, D076-3, mouse, 1:200). Appropriate fluorescent dye-labelled secondary antibodies were used (Alexa Fluor 488 and 594, 1:1000, Molecular probes). Sections were counterstained using DAPI (4',6-diamidino-2-phenylindole) and mounted in Vectashield medium (Vector laboratories, H-1200).

## In situ hybridization

Assays were run using a commercially available *LMX1A* (#540661) probe from Advanced Cell Diagnostics. Manufacturer-recommended protocols were used without modification. Sections were counterstained with hematoxylin.

## Microscopy

Zeiss LSM-Meta confocal microscope and ZEN 2009 software (Zeiss) was used to image slides from fluorescent immunohistochemical assays. Brightfield imaging of H&E stained slides was performed at 20X magnification using a Nanozoomer Digital Pathology slide scanner (Hamamatsu; Bridgewater, New Jersey). Apart from minor adjustments of contrast and brightness to the entire image, there was no additional image alteration. Figures were prepared on Adobe Illustrator.

## Cell counts

Cell counts were performed manually using Image J (SOX2/Ki67). The total number of SOX2+ or KI67+ cells relative to the total DAPI count of the EGL/rhombic lip was determined. Cells were counted by zone (VZ/SVZ/EGL) and then combined. To study the proportion of self-renewing cells and proliferative cells in the rhombic lip the following numbers of images were analyzed: Human Controls 17–19 pcw = 15 images ( $N=3$ ,  $N$  being the total number of biological samples analyzed) and DWM = 42 images ( $N=3$ ). For EGL counts a total number of 77 images over 5 DWM cases and 226 images over 22 controls were analyzed. The fastigial angle was measured with the straight-line annotation function on NDP view software. Two straight lines were drawn starting at the inner most corner of the fastigial angle and following the straight edge of each side of the angle. Angle was manually measured with a protractor after lines were determined to accurately represent the angle on the sample. The angles were classified as acute or obtuse and measured in DWM ( $N=26$ ), CVH ( $N=5$ ), Control normal samples ( $N=12$ ). To measure the extent of foliation, each foliation unit termed ‘lobuli’ was counted for all DWM, CVH and control ages.

## Statistical analysis

To determine if there was a significant difference in fastigial angles, and proportion of KI67 and SOX2+ cells between DWM and normal cerebella,  $t$  test was applied. Data is represented as mean ± SEM. Statistical analysis was done using excel. P values are listed in the figure. To determine if fetal age and DWM diagnosis were significant predictors of the number of cerebellar lobuli, multiple linear regression was performed in R specifying ~ age + diagnosis + age × diagnosis. To determine if there was a significant difference in the average number of cerebellar lobuli among regions and DWM diagnosis, ANOVA was performed in R specifying ~ lobule region + diagnosis + lobule region × diagnosis, followed by Tukey’s HSD post-hoc test for pairwise comparisons.

## Laser capture microdissection

Ten µm-thick sections for normal ( $n=2$ ) and DWM ( $n=2$ ) cerebella embedded in paraffin were collected on 2.0 µm PEN slides (Leica No.11505189). These were subsequently stained with 1% Cresyl Violet after deparaffinization with Xylene and washes in Ethanol. Laser capture microdissection was performed as described previously [18]. The microdissected tissue was transferred into RNA tissue lysis buffer provided in the High Pure FFPE RNA Isolation Kit (Roche, ref.06650775001) and RNA extraction performed

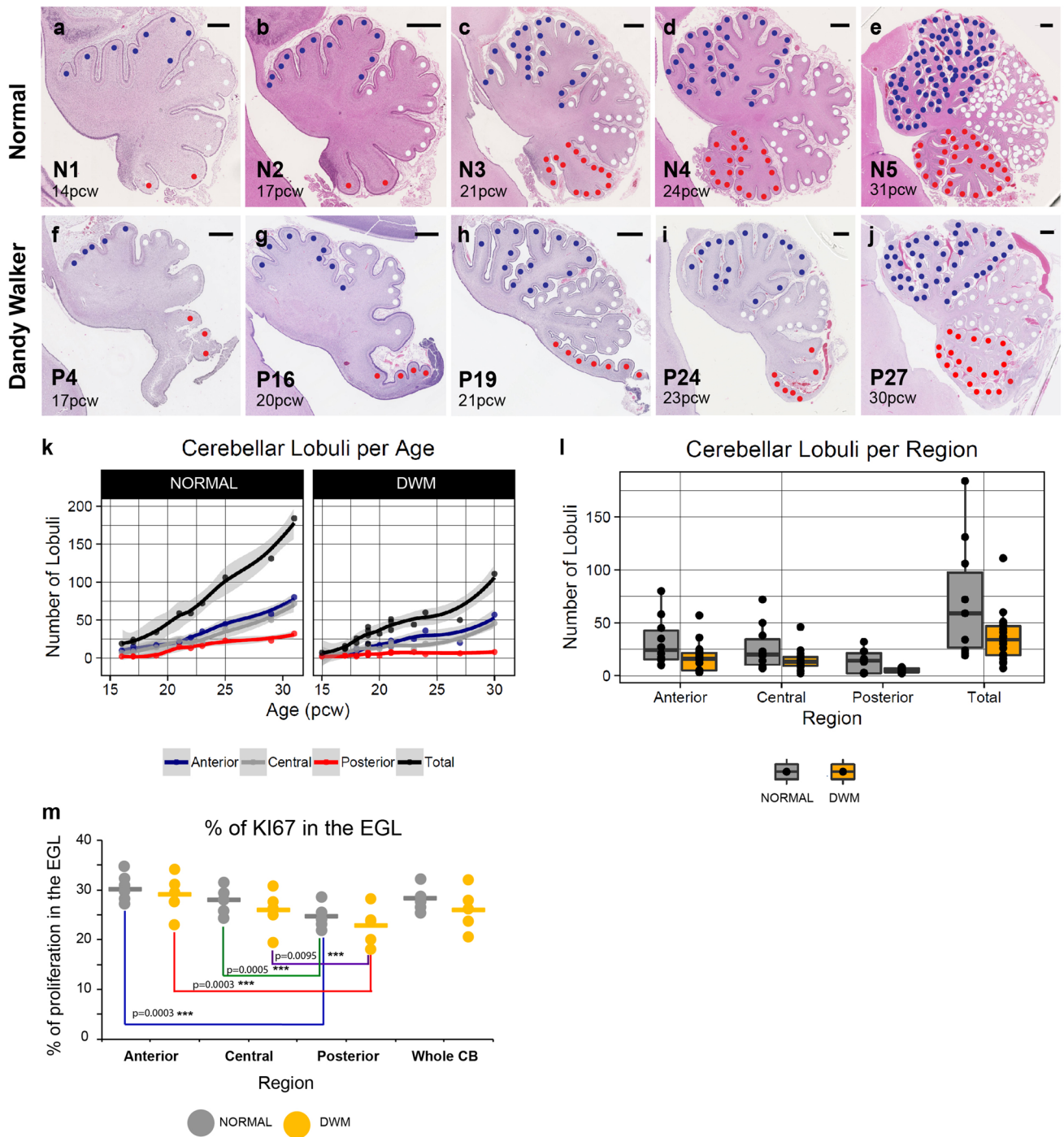
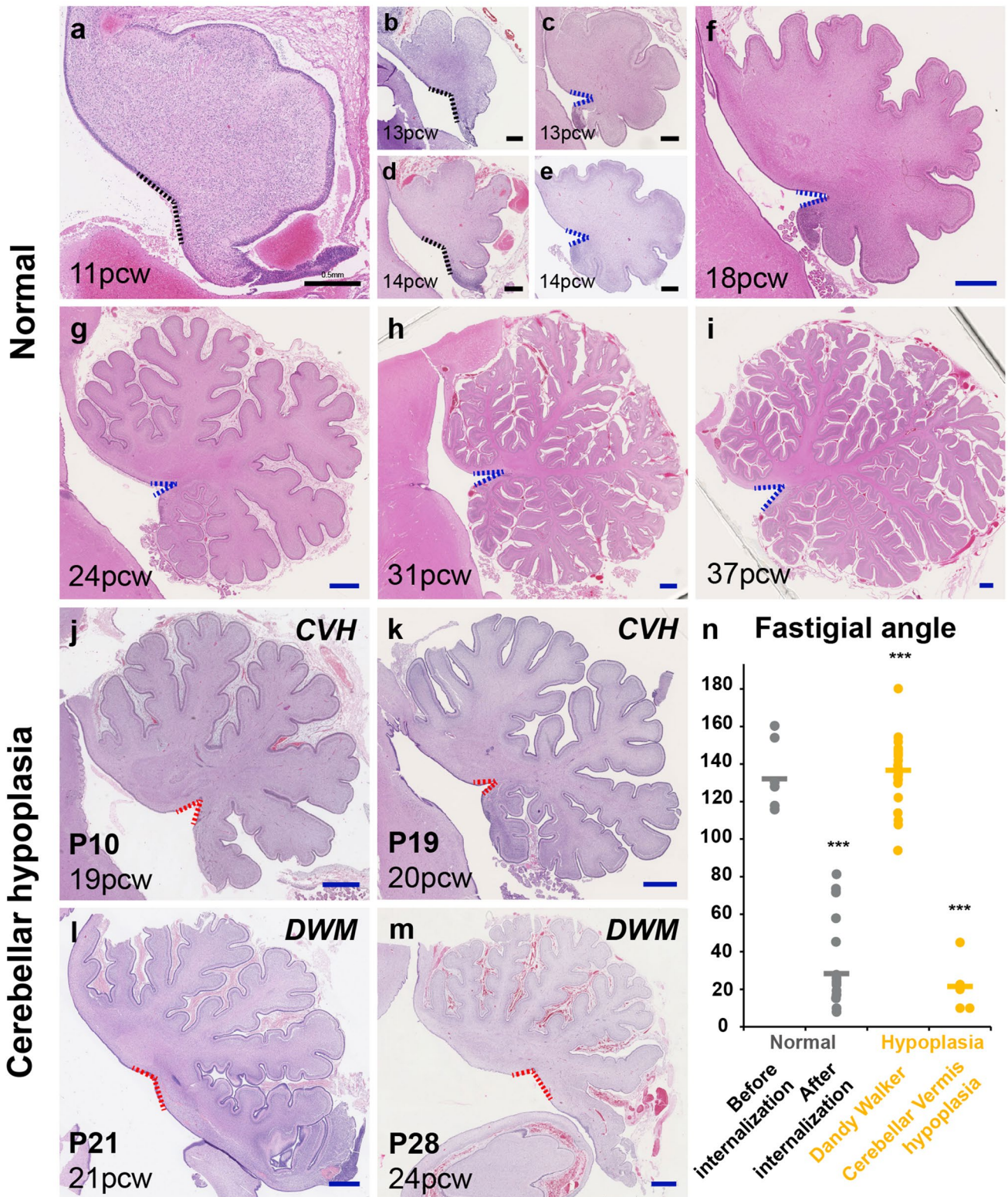


**Fig. 2** Disproportionate hypoplasia of cerebellar posterior lobules in Dandy–Walker malformation. Hematoxylin and Eosin (H&E) stained midsagittal sections of the developing normal (a–e) and DWM human cerebellum (f–j). Dots indicate number of lobuli or foliation units present at each timepoint. The anterior, central, and posterior lobes are represented by blue, white, and red dots, respectively. Distribution of the number of cerebellar lobuli per age in Control and DWM cerebellum indicates that while the posterior lobe grows at a much slower rate in normals, the posterior lobe remains dispro-

tionately hypoplastic in DWM (k). Number of lobuli by both region and diagnosis in normal control (grey) and DWM (yellow) cerebella indicates disproportionate posterior lobule hypoplasia in DWM (l). KI67 immunohistochemical assays indicate no significant difference in proliferation between normal and DWM in respective lobes (*t* test), although proliferation is significantly lesser in the posterior lobes when compared to the anterior lobe within the normal and DW cerebellum. Mean is represented by lines, while dots represent individual data points (m). Scale bar = 1 mm (a–j)



using manufacturer-recommended protocols. The Agilent Bioanalyzer 600 Pico Kit was used to assess RNA quality (DV200 > 74 for all samples).

**RNA sequencing and analysis**

Library preparation and sequencing were performed by the Applied Genomics, Computational & Translational Core at

**Fig. 3** Cerebellum in Dandy–Walker malformation displays a characteristically blunt and obtuse fastigial angle. **a–i** H&E stained midsagittal sections show the progression of the fastigial angle in a normal cerebellum as it changes from obtuse (black dashes) to acute (blue dashes). The fastigial angle is not age-dependent, but dependent on the internalization of the rhombic lip and growth of the posterior lobe around 14pcw (**b–e**). **j, k** Cerebellar vermian hypoplasia (CVH) cases possess an acute fastigial angle (red dashes), suggesting the rhombic lip is not disrupted until after internalization. **l, m** DWM cases demonstrate a blunt and obtuse fastigial angle (red dashes). **n** Graph comparing the fastigial angle (*y*-axis) in DWM (yellow), CVH (yellow), and normal cerebella (grey) in a grouped-column scatterplot. The fastigial angle becomes significantly acute in the normal cerebellum after RL internalization (*t* test;  $p < 0.0001$ ). In the DWM cerebellum the fastigial angle is only similar to normal pre-internalization cerebella but remains significantly obtuse compared to normal post-internalization cerebella (*t* test;  $p < 0.0001$ ) and CVH whose fastigial angles are acute themselves ( $p < 0.0001$ ; compared to DWM). Mean is represented by lines, while dots represent individual data points. Scale bar = 0.5 mm (black) and 1 mm (blue)

Cedars Sinai. Sequencing libraries were prepared using the TruSeq RNA Exome Prep Kit (Illumina) and 50 ng of total RNA, according to the manufacturer’s protocol. Indexed libraries were pooled and loaded onto an Illumina NovaSeq. Paired-end reads (100 bp) were aligned to the Human reference genome (GRCh38) using STAR v2.5.3a [14], gene counts were summarized using featureCounts v1.6 [24], and gene-level differential expression was analyzed using DESeq2 [26]. Transcripts per million were calculated using TPMCalculator [33]. Significant results are reported as Benjamini–Hochberg adjusted *p* values.

## Results

### Upward rotation of cerebellar vermian in Dandy Walker malformation

We studied the histopathology of a total of 31 cerebellar malformation cases between 15 and 34 post-conception weeks (pcw) from multiple centers (Suppl. Fig. S1, 2; Suppl. Table S1; online resource). Centers independently diagnosed 26 cases as DWM and 5 as CVH following an initial ultrasound followed by fetal MRI, with diagnosis confirmed by pathology. For 6 DWM cases we obtained imaging files and performed morphobiometric analyses of the cerebellum, measuring: a) vermian antero-posterior diameter (APD), b) vermian cranio-caudal diameter (CCD) and c) the tegmento-vermian angle (TVA), as defined previously [11, 35] (Fig. 1d–f; table). The vermian APD and CCD for all of the cases studied was below the 5th percentile, while the TVA was wider in all cases indicating that the cerebellar morphobiometry of our cases deviated significantly from normal [11, 35].

### The posterior vermian is disproportionately hypoplastic in DWM

Hypoplasia of the cerebellar vermian is a principal feature of DWM, manifested as reduced cerebellar volume and foliation. We measured the extent of foliation by counting the number of lobuli across the developing normal and DWM cerebellum [17] (Fig. 2). We define lobuli as the smallest foliation unit within a larger lobule, which in turn constitutes the 10 lobules normally present within the anterior, central and posterior lobes. In normal cerebella, the anterior, central and posterior lobes do not grow concurrently [18]. Notwithstanding variability, growth and foliation of the anterior and central lobes precedes that of the posterior lobe. There is no significant growth of the posterior lobe between 14 and 18 pcw. After 18 pcw; however, the posterior lobe grows exponentially (Fig. 2a–e, k). In the DWM cerebella, although hypoplasia was seen across lobes, the posterior lobe was disproportionately hypoplastic and its growth did not catch up with the controls resulting in significantly reduced foliation, even as the anterior and central lobes grew (Fig. 2f–j, k, l). In the CVH cases studied, the number of lobuli were fewer compared to age-matched normal samples but greater than the DWM cerebella. A multiple linear regression was calculated to predict the number of cerebellar lobuli based on fetal age and diagnosis. A significant regression equation was found [ $F(3, 108) = 33.25, p = 2.65 \times 10^{-15}, R^2 = 0.47$ ]. The number of lobuli increased by 5.22 for each postconceptional week with a significant main effect, while there was a significant interaction between fetal age and diagnosis such that fetuses diagnosed with Dandy Walker malformation had 2.27 fewer lobuli for each postconceptional week compared to controls. We found a statistically significant difference in the number of lobuli by both region [ $F(2) = 8.28, p = 0.0005$ ] and by diagnosis [ $F(1) = 13.64, p = 0.0004$ ]. A Tukey post-hoc test revealed that the posterior region had significantly fewer lobuli compared to anterior and central regions. Diagnosis was also significant, with Dandy Walker malformation resulting in 11.54 fewer lobuli on average compared to controls across regions.

### Reduced proliferation of posterior-lobe granule neuronal precursors in DWM cerebellum

GNP proliferation in the external granule layer (EGL) drives cerebellar growth during mid-gestation [29]. Our analysis indicates that in normal developing cerebella, the level of GNP proliferation in the posterior lobe of the normal developing cerebellum was significantly lower than the anterior or central lobes (Fig. 2m; *t* test;  $p < 0.0005$ ). Although this trend was conserved in the DWM cerebellum, reduction in posterior EGL proliferation was not significantly lower than in normal, indicating that reduced EGL proliferation during

the stages evaluated was likely not primarily responsible for hypoplasia of the posterior lobe ( $t$  test;  $p = 0.75$ ).

### The DWM cerebellum displays a blunt fastigial recess

The fastigial recess is a projection of the fourth ventricle into the cerebellar ventricular zone surface at the junction of the anterior and posterior vermis (Fig. 3a–i, dashed lines). During early embryonic and fetal development, when the rhombic lip is small compared to the ventricular zone, the nascent fastigial angle is wide and obtuse. However, we noted that as the rhombic lip normally expands and internalizes leading to the growth of the posterior-most lobule, the fastigial angle became sharp, narrow and acute (Fig. 3a–i, n). In DWM samples, we observed conspicuous blunting and flattening of the fastigial recess, such that the angle remained obtuse even at 30 pcw (Fig. 3l–n; Suppl. Fig. S1, online resource). Therefore, we posit that in DWM cases, rhombic lip development is disrupted, prior to internalization, before 14 pcw. In contrast, all 5 CVH cases displayed sharp, acute fastigial angles, despite considerable posterior hypoplasia (Fig. 3j, k), suggesting cerebellar developmental disruption likely occurred only after rhombic lip internalization (after 14 pcw). Later disruption also explains why the CVH posterior lobe is often considerably more developed compared to DWM.

### A tail-like sign is a conspicuous feature of human DWM

We previously defined an expanded trailing posterior vermis ‘tail sign’ to distinguish DWM from other cerebellar hypoplasias in MRI analyses [8]. We now show that this tail sign, discernable in fetal and postnatal MRI (Fig. 4a, b), is readily observed during autopsy (Fig. 4c, d; Suppl. Fig. S2, online resource) and in histological sections (Fig. 4e–k, red arrowhead; Suppl. Fig. S1, online resource). We also show that the DWM tail is composed of a partially formed unpaired lobule that bears a striking resemblance to the unpaired posterior lobule we previously reported in the postnatal *Foxc1<sup>hih/hih</sup>* mutant mouse [20]. Every DWM sample analyzed in this study had an unpaired posterior lobule, while ~75% displayed a ‘tail sign’, where the outer limit of the posterior lobe extended beyond the circumference of the cerebellum as a whole (Fig. 4e–k). Underdevelopment of the posterior vermis was accompanied by abnormal rhombic lip morphology. While in approximately half of our samples, the partially formed posterior lobule had a terminal hypercellular tail-like rhombic lip, in ~30% of our samples, the rhombic lip was completely absent, confirming our prior preliminary that the rhombic lip is essential for the growth and maintenance of the posterior vermis [18] (Fig. 4h). The presence of an incipient fastigial recess and a tail-like rhombic lip

in DWM samples compared to age-matched control samples emphasizes aberrant development of the rhombic lip in DWM.

### Aberrations in rhombic lip development are likely responsible for posterior vermis hypoplasia in DWM

To define the extent of abnormal rhombic lip development in DWM samples, we performed a series of histopathological and molecular analyses. We previously identified the human rhombic lip (Fig. 5, red arrowheads) as a highly proliferative stem cell zone that originates as an elongated tail-like protrusion with unique human-specific substructure. Around 14 pcw, the rhombic lip internalizes into the posterior lobule promoting its growth throughout gestation [18]. In this study, KI67 immunohistochemistry revealed significantly reduced DWM rhombic lip cell division (Fig. 5a–d, h) accompanied by a significant reduction in the proportion of self-renewing SOX2-expressing progenitors (Fig. 5e–g, i). Reduced KI67+ and SOX2+ populations were evident in both proliferative compartments of the rhombic lip, the RL ventricular zone (RL<sup>VZ</sup>, red asterisk) and RL subventricular zone (RL<sup>SVZ</sup>, yellow asterisk). Reductions were more pronounced in the RL<sup>VZ</sup>, where most of the undifferentiated self-renewing radial glia reside (Fig. 5h, i).

Despite reduced proliferation in the DWM rhombic lip, the region was remarkably hypercellular. Expression of classic rhombic lip markers including *LMX1A* and *PAX6* shows that the region retained its rhombic lip-like identity (Fig. 5j–l). However, increased numbers of TBR2+/KI67– cells in the DWM RL<sup>SVZ</sup> demonstrated precocious differentiation of rhombic lip progenitors into TBR2+ unipolar brush cells (UBC) which ectopically accumulated within the residual DWM rhombic lip (Fig. 5k, l).

During normal development, the RL<sup>VZ</sup> and RL<sup>SVZ</sup> are separated by a distinct barrier composed of an extensive vascular bed [18] (Fig. 5n, white arrowheads). Since abnormal vascular development has been linked to cerebellar malformations including DWM [4], we sought to examine the rhombic lip vasculature in the DWM cerebellum. We found that displacement of proliferating cells within the rhombic lip leading to a disruption in the laminar structure was associated with a concomitant variable rearrangement of the vascular bed in DWM samples, including pockets of KI67+ cells within the RL<sup>SVZ</sup> surrounded by vascular cells (Fig. 5m, o, p, white arrowheads). We cannot determine whether this alone led to a reduction in progenitor proliferation and self-renewal, but the concurrence is suggestive.



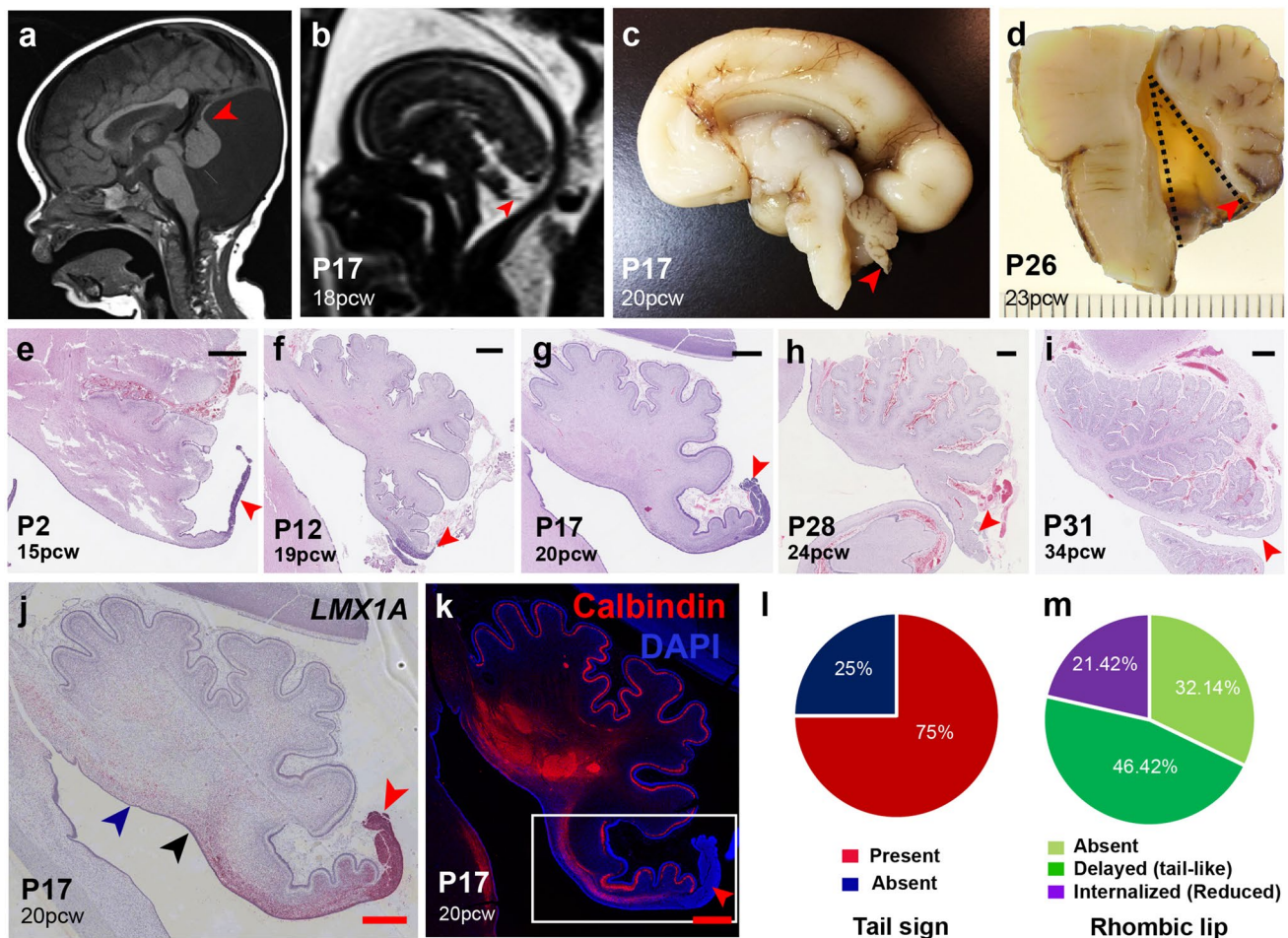


**Fig. 4** ‘Tail Sign’ is a conspicuous feature of Dandy–Walker malformation. Midsagittal MRI scans of postnatal (a) and fetal DWM (b) show a characteristic ‘tail sign’ (red arrowhead) that is also conspicuous during autopsy (c, d) and histological analysis (e–k). *LMX1A* (j) and Calbindin (k) expression indicate that the tail sign is composed of non-internalized rhombic lip (red arrowhead) attached to a partially formed unpaired posterior lobule. Ventricular zone (blue arrowhead) and fastigial recess (black arrowhead) are also marked (j). Pie

charts showing the presence of the tail-sign in the majority (75%) of DWM cases studied (l), and the developmental status of the rhombic lip in each of these same cases, with the rhombic lip being absent in 32% of the cases studied, while an underdeveloped reduced rhombic lip was seen in 46% of cases studied. Only 21% of cases analyzed had an internalized albeit reduced rhombic lip (m). Scale bar = 1 mm (e–k)

### Genes associated with the regulation of normal cell division are downregulated in the DWM rhombic lip

To define molecular programs underlying the histological phenotypes, we performed an unbiased molecular analysis of the human DWM vs normal rhombic lip. Specifically, we profiled the DWM rhombic lip transcriptome using laser-capture microdissection to isolate the rhombic lip from two archival DWM cases (Fig. 6a, black outline) and two normals, then performing RNA-sequencing. We also generated data from age-matched control samples that were processed in an identical fashion (Suppl. Table S2, online resource).

Differential expression analysis between the normal and DWM rhombic lip identified 308 and 265 genes that were up- and downregulated, respectively (Fig. 6b; Suppl.

Table S3, online resource). Upregulated genes included UBC markers, such as *GRIA2*, *RPH3A*, *CALD1*, *ANK3*, consistent with the increased numbers of TBR2+ cells in the DWM RL detected histologically (Fig. 6c, d). Significantly, downregulated genes were associated with proliferation and self-renewal, including proliferation markers (*MKI67*, *PCNA*, *CCND1*); apical polarity proteins (*PROM1* and *CRB2*) and mitogenic factors (*YAP1* and *NOTCH1*). Genes involved in the regulation of mitosis, including those implicated in microcephaly were also significantly downregulated (*ASPM*, *STIL*, *CENPN*). Expression of genes associated with rhombic lip identity, such as *OLIG3*, *RSP01*, and *WNT2B*, were also reduced. Interestingly, *PROKR1*, a gene that promotes angiogenesis was also downregulated in the DWM rhombic lip.

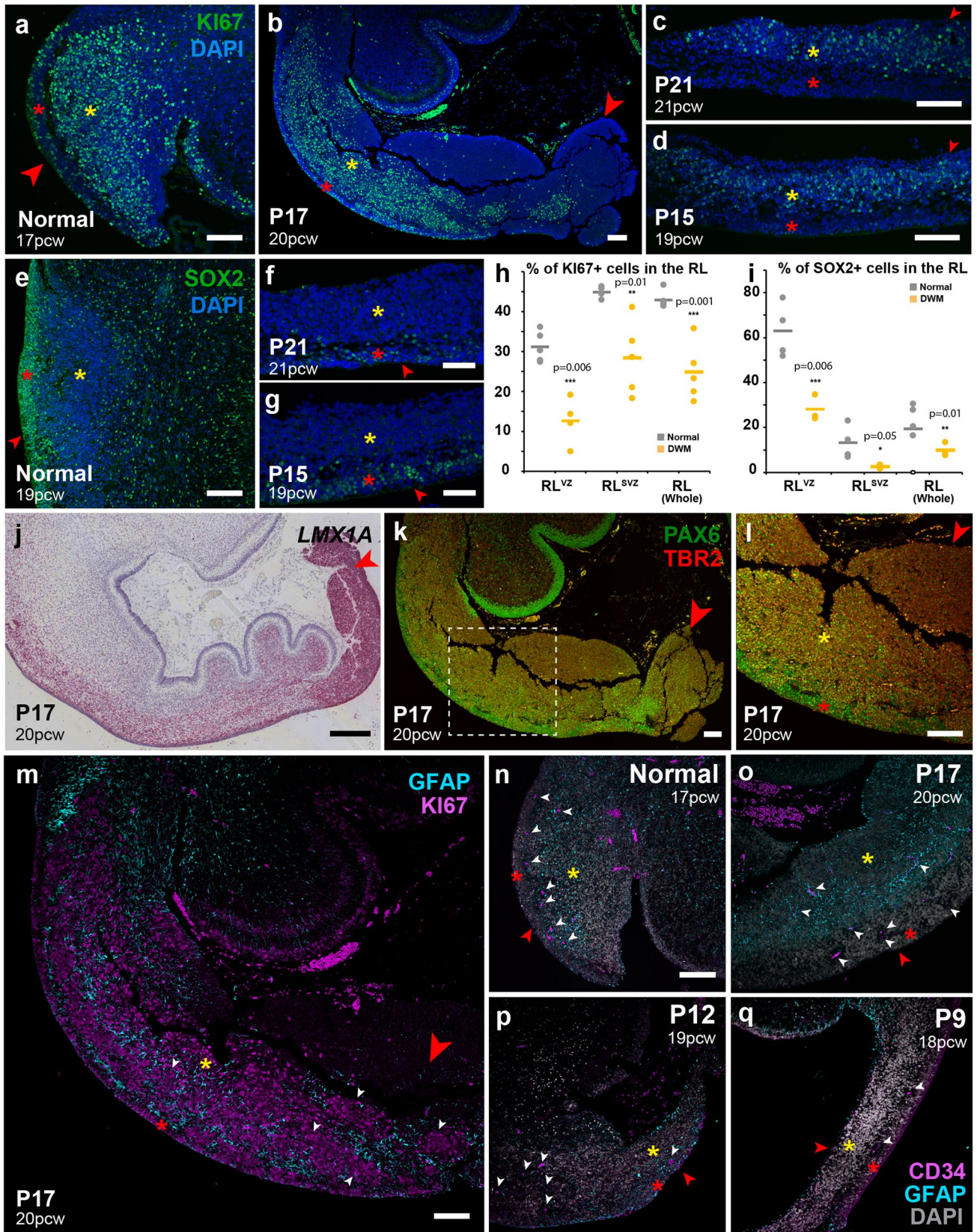


**Fig. 5** Histopathology of aberrant rhombic lip development in Dandy–Walker malformation. Immunohistochemistry and in situ hybridization assays data on the human cerebellar rhombic lip (red arrowheads, **a–g, j–q**). KI67 immunostaining in the RL<sup>VZ</sup> (red asterisk) RL<sup>SVZ</sup> (yellow asterisk) of normal (**a**) and DW cerebella (**b–d**). Graph comparing percentage of Ki67+ cells (y-axis) in the RL<sup>VZ</sup>, RL<sup>SVZ</sup> and the whole RL (**h**). SOX2 immunostaining in the RL<sup>VZ</sup>, RL<sup>SVZ</sup> of normal (**e**) and DW cerebella (**f, g**). Graph comparing percentage of SOX2+ cells (y-axis) in the RL<sup>VZ</sup>, RL<sup>SVZ</sup> and the whole RL (**i**). Tail-like structure retains rhombic lip identity as evinced by *LMX1A* ISH (**j**), PAX6, and TBR2 immunohistochemistry (**k, l**). **l** is an inset of **k** denoted by a white dashed box. Marked increase in TBR2 staining in the RL<sup>SVZ</sup> shows buildup of precociously differentiated UBCs (**l**). GFAP-KI67 staining in the DWM RL (**m**). GFAP-CD34 staining for the rhombic lip vascular bed (white arrowheads) indicates its organized arrangement in normal (**n**) while being displaced and disorganized in the DWM rhombic lip (**m, o–q**). In Graphs **h** and **i**, Mean is represented by lines, while dots represent individual data points (*t* test; *p* < 0.05). Scale bar = 0.5 mm (black) and 100 μm (white)

Our transcriptome data buttresses our histopathological data which indicates a significant reduction in the rhombic lip progenitor pool, either due to reduced proliferation and self-renewal or precocious differentiation, with a potential link to vascular insults.

## Discussion

When initially described, DWM pathology was thought to be caused by impaired cerebrospinal fluid (CSF) dynamics [7, 12, 32]. This hypothesis has been discredited, in part due to findings in human genetics and modeling in mice, which pointed to primary disruptions in cerebellar development [2, 20, 21]. Yet, a comprehensive analysis of developing human DWM samples has never been undertaken previously. Here we present the first large study of developing human cerebellar malformation samples from 15 to 34 pcw, including 26 DWM samples, 5 CVH samples and 23 age-matched normal control samples. We acknowledge that each human sample represents a snapshot of development; we lack data from its earlier stages of development and cannot predict the outcome if development had proceeded. However, our comprehensive analysis of this large series of samples implicates an insult to the human cerebellar rhombic lip (~ < 14 pcw) as a primary cause. Compromised regulation of proliferation and differentiation of the stem cell population in this important transient progenitor zone correlates with an extremely hypoplastic and dysplastic posterior cerebellar vermis with hallmark features of DWM.

## Model for Dandy–Walker malformation in humans

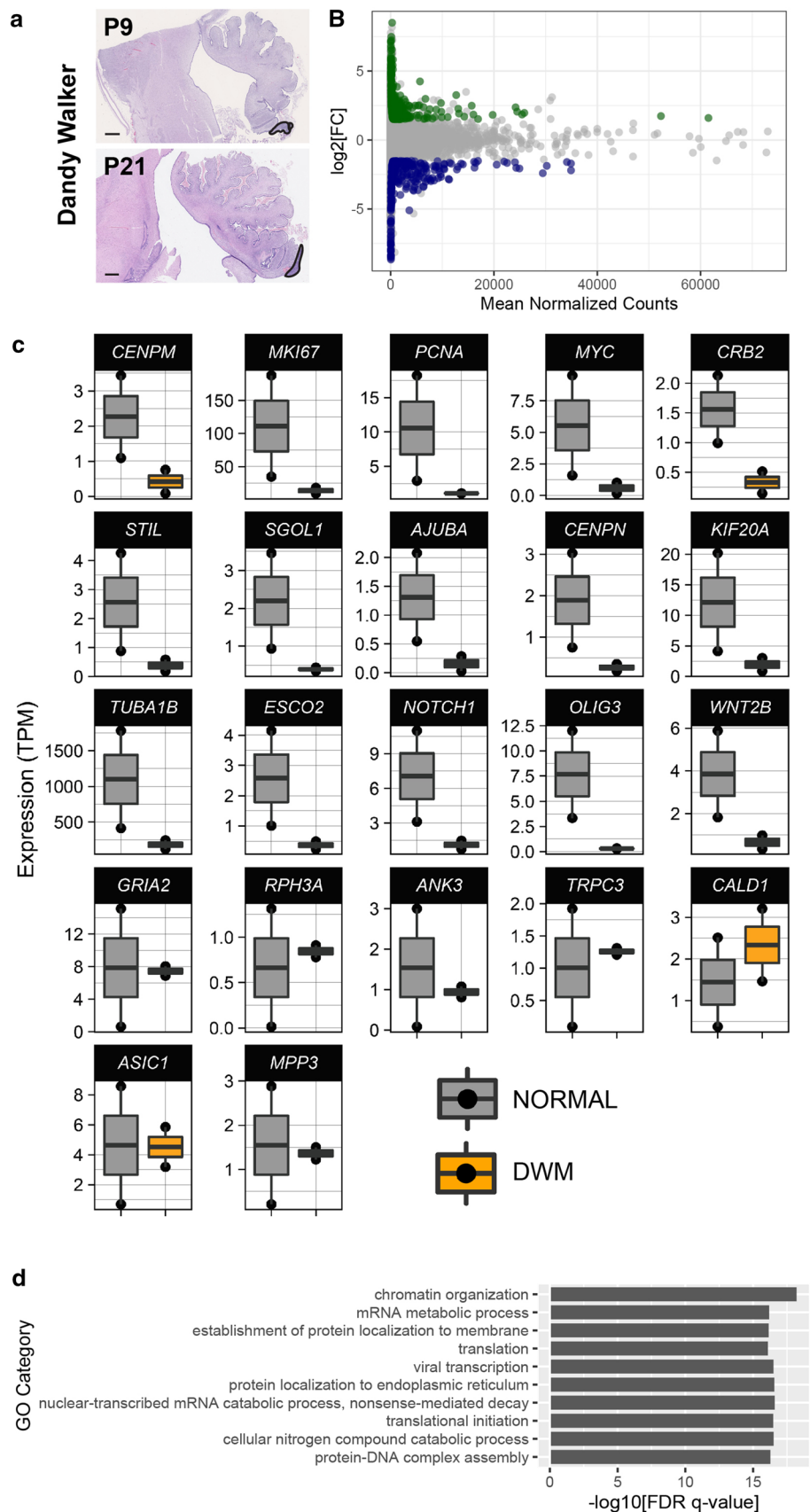
The human cerebellum undergoes rapid growth during the third trimester [25]. This growth, manifested by an increase

in volume and foliation, is driven by the exponential growth of GNPs in the EGL, with peak proliferation occurring during 26–32 pcw [29]. Insults including premature birth reduce this EGL proliferation resulting in reduced cerebellar volume [25, 34]. Our data show that in DWM the volume of the vermis, particularly the posterior vermis, is significantly reduced, at the earliest by 15 pcw, several weeks before the onset of peak EGL proliferation indicating an earlier derailment of development. Older, late-gestation DWM samples have a well-developed and considerably foliated anterior lobe (Figs. 2i, j, 3h, i; Suppl. Figure S1, P23–P31, online resource) suggesting peak EGL proliferation likely remains unaffected and inferior vermian hypoplasia is induced by an earlier insult. Several aspects of our current analyses point to a disrupted rhombic lip as a primary cause of DWM, with the timing of disruption distinguishing DWM from CVH.

The rhombic lip in both mice and humans, is a transient, dorsally located highly proliferative stem cell zone giving rise to all cerebellar glutamatergic populations, including glutamatergic cerebellar nuclei neurons, GNPs and unipolar brush cells (Fig. 7; 8pcw). In both species, the early rhombic lip is similar. However, as development progresses the similarity between the two homologous structures across species diminishes. In mice, the rhombic lip remains small, lacks structural compartmentalization and disappears before key phases of cerebellar growth and foliation. In humans, as the first signs of cerebellar foliation appear around 11 pcw, the rhombic lip compartmentalizes into a RL<sup>VZ</sup> and RL<sup>SVZ</sup>, with each proliferative zone separated by a distinct vascular–glial region composed of GFAP+ and CD34+ cells [18]. At this stage, the human rhombic lip normally resembles a tail with an outer limit extending beyond the circumference of the cerebellar lobes (Fig. 7; 11 pcw). With gradual increase in cerebellar volume, particularly in the posterior lobe, the outer limit of the human posterior lobe and rhombic lip align normally by 13 pcw (Fig. 7; 13 pcw, blue line). As the posterior lobe continues to grow beyond the outer limit of the rhombic lip (black arrows), the rhombic lip is internalized and forms a pool of cells in the posterior-most lobule (Fig. 7; 14 and 17 pcw). Growth of the posterior lobe driven by the rhombic lip and its involution concomitantly causes the fastigial recess to sharpen and become narrow (Fig. 7, red dashed lines).

Our comprehensive analysis of developing DWM samples suggests that while EGL formation and proliferation are unaffected during early stages, progenitor proliferation and self-renewal in the DWM rhombic lip is significantly reduced (Fig. 7, DW 11–14 pcw). Indeed, absence or reduction in rhombic lip size is accompanied by disproportionate hypoplasia of the posterior lobules in all of our samples, even as early as 15 pcw. We posit that earlier damage to the rhombic lip, due to vascular or other extrinsic disruptions or aberrations in intrinsic cellular programming reduces

**Fig. 6** Transcriptional profiling of the Dandy–Walker malformation rhombic lip. **a** H&E stained midsagittal sections of the DWM cerebellum depicting the rhombic lip progenitor zone isolated by laser-capture microdissection. **b** Scatterplot of the logarithmic fold changes (y-axis) between DWM and control normal rhombic lip versus the mean of normalized counts (x-axis). Genes upregulated in the DWM rhombic lip are shown in green and downregulated are shown in blue. **c** Box plots of notable differentially expressed genes between normal (grey) and DWM (yellow). Gene expression is measured in transcript per million (TPM). **d** Gene ontology (GO) enrichment analysis among differentially expressed genes. The top 10 GO categories are shown. Scale bar = 1 mm (a, b)



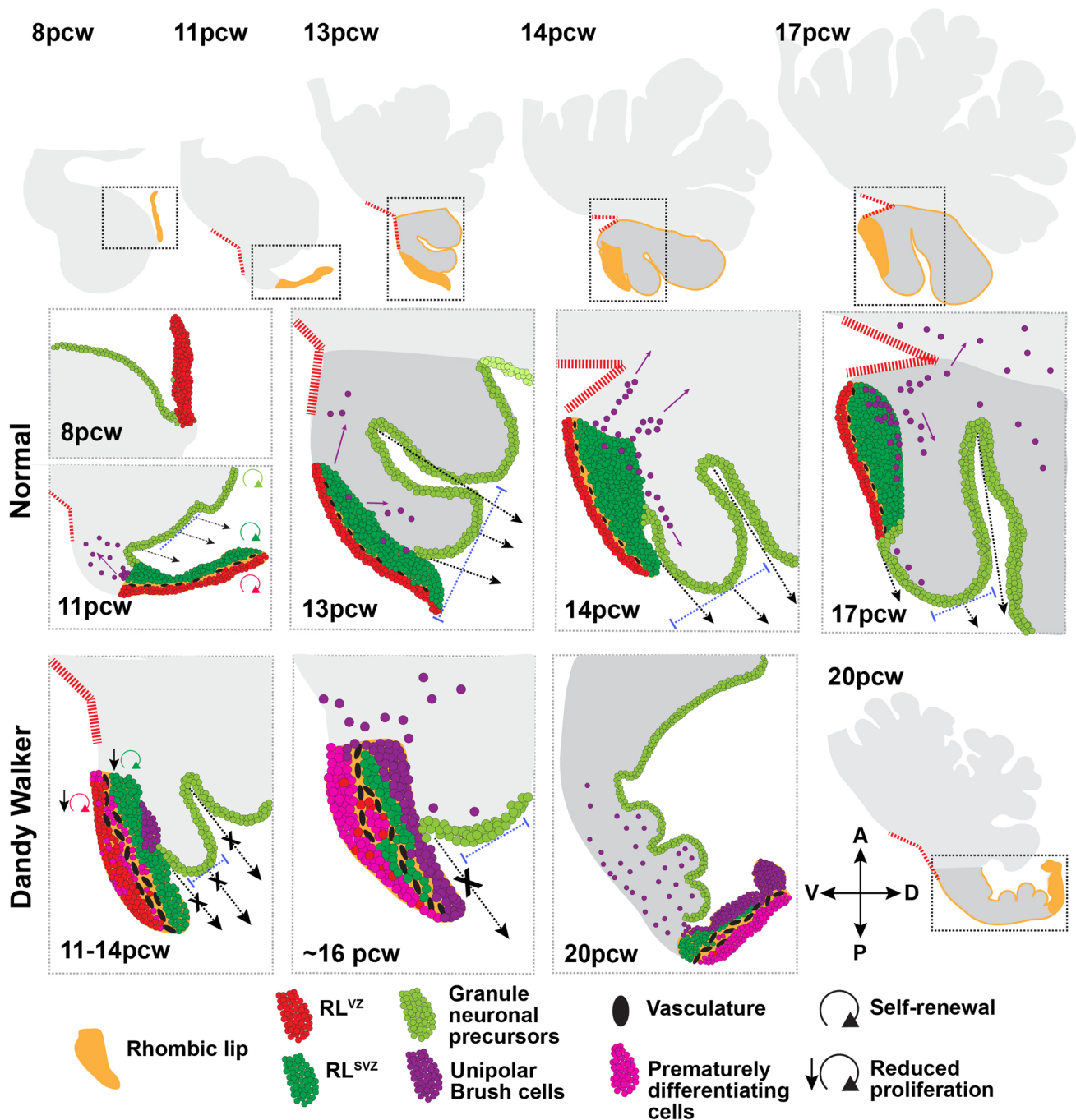


**Fig. 7** Developmental model for Dandy–Walker malformation in humans. Model for the internalization of the rhombic lip (yellow), and the subsequent sharpening of the fastigial angle (red dashes). During normal development, the rhombic lip compartmentalizes into a RL<sup>VZ</sup> (red) and RL<sup>SVZ</sup> (dark green) separated by a vascular bed (black). The rhombic lip feeds granule neuronal precursors (light green) into the external granule layer promoting growth of the posterior vermis (dark grey). The rhombic lip also produces unipolar brush cells (purple) that stream into the multiple cerebellar lobules. During early development the RL extends beyond the perimeter of the posterior lobule (blue dashes). Outward growth of the posterior-most

lobule (black arrowheads) causes the internalization of the rhombic lip and a concomitant blunting of the fastigial angle (red dashes). In the DWM cerebellum, insults, such as vascular disruptions result in reduced self-renewal and premature differentiation of rhombic lip progenitors (11–16pcw, magenta), which further leads to reduced growth of the posterior vermis, resulting in the fastigial angle remaining obtuse. Prematurely differentiated UBCs build up in the DWM rhombic lip (16–20pcw, purple). Reduced growth of the posterior vermis correlates with failure of the rhombic lip to internalize, resulting in tail-like structure (Dandy–Walker, 20pcw, box)

progenitor number. In addition, we observe premature differentiation of rhombic lip progenitors into UBCs, further contributing to the progenitor pool depletion and its early regression. Early loss of the DWM rhombic lip also decreases production of posterior lobe GNPs, leading to underdevelopment of the posterior lobe which fails to grow beyond the outer limit of the rhombic lip, resulting in the formation of a partially formed posterior lobule with a trailing tail-like structure (Fig. 7, DW 16–20 pcw).

Underdevelopment of the posterior vermis ensures that the fastigial angle fails to narrow and instead remains wide and obtuse. Our transcriptomic analysis indicates that many of the genes downregulated in the DWM rhombic lip play a role in polarity, progenitor expansion and normal progression of cell division. In fact, some downregulated markers have been implicated in microcephaly, where progenitor depletion results in reduced cerebral volume [15].

We posit that there are distinct underlying pathogenetic mechanisms for DWM and CVH. In both DWM and CVH, cerebellar volume is reduced, and the posterior-most lobule is partially formed (Suppl. Fig. S1, P10 and P18, online resource). However, in CVH, the rhombic lip is internalized, similar to control samples and not ‘tail-like’. Concurrently in CVH, the fastigial angle is acute suggesting that disruption of rhombic lip development likely occurs only after it is internalized following the early growth of the posterior vermis. Hence, even though the posterior-most lobule remains partially formed in CVH, it is more developed than in DWM. This phenotype is recapitulated in the hypomorphic *Foxc1* DWM mouse model we previously described, where the initial period of rhombic lip development is largely normal but as development proceeds, cells that build the posterior-most region are either underproduced and/or mis-migrate, leading to the formation of a partially formed posterior lobe [20]. Since both imaging and histological information was available for 6 samples, we confirmed that the DWM imaging “tail-sign” [8] clearly correlates with a disrupted rhombic lip and severely compromised posterior cerebellar development in DWM. Further studies of additional CVH samples are needed to confirm the pathological and molecular basis of aberrant rhombic lip development including whether this tail sign is specific to DWM. Prospective studies of affected developmental cases diagnosed post-imaging will provide currently missing information regarding developmental outcome.

Our recent discovery of key normal human-specific cerebellar developmental programs, particularly human rhombic lip development, underscores the importance of detailed histopathological and molecular developmental analyses of human cerebellar malformations [3, 18]. Our analysis of the first large series of developmental samples has yielded significant new insights into the pathogenesis of DWM defining an early (~ < 14 pcw) insult to the cerebellar rhombic lip

as central to DWM pathology, which likely distinguishes DWM from CVH and may improve diagnostic and prognostic information for affected families. Similar developmental studies are clearly warranted for other human brain malformations as multiple features of human brain development diverge from common model systems, particularly mice.

**Supplementary Information** The online version contains supplementary material available at <https://doi.org/10.1007/s00401-021-02355-7>.

**Acknowledgements** We thank the staff at Human Developmental Biology Resource and Birth Defects Research Laboratory; Xuemei Deng, Conrad Winter, Jennifer Forrer (Seattle Children’s Hospital) and Armelle De Mauduit (APHP) for their technical help and support.

**Author contributions** PH and KJM conceived, designed, and oversaw the execution of the study. Data collection and analysis was performed by PH, TS, SB, DD, AHS, JM, DD, MD, AET, BDD, and JTP. Samples and radiological data were provided by SB, LM, KM, OO, FG, IAG, HAB, RR, JRS, DK, FR, GP, NR, CDG, and ES. KAA designed and oversaw LCM and RNA-seq data collection and analysis. PH and KJM wrote the first draft. All authors reviewed and critiqued the manuscript.

**Funding** National Institutes of Health R01 NS080390 and R01 NS095733 (KJM). National Ataxia Foundation Young Investigator Research Grant, Brain and Behavior Research Foundation Young Investigator Award #28956, and Franklin Research Award by the American Philosophical Society (PH).

**Data availability and materials** Normal human material was provided by the Joint Medical Research Council/Wellcome (MR/R006237/1) HDBR ([www.hdbr.org](http://www.hdbr.org)), and the BDRL, University of Washington (NIH R24 HD000836 awarded to IAG). Human tissue used in this study was covered by a material transfer agreement between SCRI and HDBR/BDRL. Sequence data will be available upon request.

## Declarations

**Conflict of interest** The authors declare no competing interests.


## References

1. Aldinger KA, Doherty D (2016) The genetics of cerebellar malformations. *Semin Fetal Neonatal Med* 21:321–332. <https://doi.org/10.1016/j.siny.2016.04.008>
2. Aldinger KA, Lehmann OJ, Hudgins L, Chizhikov VV, Bassuk AG, Ades LC (2009) FOXC1 is required for normal cerebellar development and is a major contributor to chromosome 6p25.3 Dandy-Walker malformation. *Nat Genet* 41:1037–1042. <https://doi.org/10.1038/ng.422>
3. Aldinger KA, Thomson Z, Phelps IG, Haldipur P, Deng M, Timms AE et al (2021) Spatial and cell type transcriptional landscape of human cerebellar development. *Nat Neurosci*. <https://doi.org/10.1038/s41593-021-00872-y>
4. Aldinger KA, Timms AE, Thomson Z, Mirzaa GM, Bennett JT, Rosenberg AB et al (2019) Redefining the etiologic landscape of cerebellar Malformations. *Am J Hum Genet* 105:606–615. <https://doi.org/10.1016/j.ajhg.2019.07.019>

5. Barkovich AJ, Millen KJ, Dobyns WB (2009) A developmental and genetic classification for midbrain-hindbrain malformations. *Brain* 132:3199–3230. <https://doi.org/10.1093/brain/awp247>
6. Barkovich AJ, Millen KJ, Dobyns WB (2007) A developmental classification of malformations of the brainstem. *Ann Neurol* 62:625–639. <https://doi.org/10.1002/ana.21239>
7. Benda CE (1954) The Dandy-Walker syndrome or the so-called atresia of the foramen Magendie. *J Neuropathol Exp Neurol* 13:14–29. <https://doi.org/10.1093/jnen/13.1.14>
8. Bernardo S, Vinci V, Saldari M, Servadei F, Silvestri E, Giancotti A et al (2015) Dandy-Walker Malformation: is the ‘tail sign’ the key sign? *Prenat Diagn* 35:1358–1364. <https://doi.org/10.1002/pd.4705>
9. Cater SW, Boyd BK, Ghate SV (2020) Abnormalities of the fetal central nervous system: prenatal US diagnosis with postnatal correlation. *Radiographics* 40:1458–1472. <https://doi.org/10.1148/rg.2020200034>
10. Chapman T, Mahalingam S, Ishak GE, Nixon JN, Siebert J, Dighe MK (2015) Diagnostic imaging of posterior fossa anomalies in the fetus and neonate: part 2, Posterior fossa disorders. *Clin Imaging* 39:167–175. <https://doi.org/10.1016/j.clinimag.2014.10.012>
11. Conte G, Milani S, Palumbo G, Talenti G, Boito S, Rustico M et al (2018) Prenatal brain MR imaging: reference linear biometric centiles between 20 and 24 gestational weeks. *AJNR Am J Neuroradiol* 39:963–967. <https://doi.org/10.3174/ajnr.A5574>
12. Dandy W, Blackfan K (1914) Internal hydrocephalus: an experimental, clinical and pathological study. *Am J Dis Child* 8:406–482
13. Delahaye A, Khung-Savatovsky S, Aboura A, Guimiot F, Drunat S, Alessandri JL et al (2012) Pre- and postnatal phenotype of 6p25 deletions involving the FOXC1 gene. *Am J Med Genet A* 158A:2430–2438. <https://doi.org/10.1002/ajmg.a.35548>
14. Dobin A, Davis CA, Schlesinger F, Drenkow J, Zaleski C, Jha S et al (2013) STAR: ultrafast universal RNA-seq aligner. *Bioinformatics* 29:15–21. <https://doi.org/10.1093/bioinformatics/bts635>
15. Gabriel E, Ramani A, Altinisik N, Gopalakrishnan J (2020) Human brain organoids to decode mechanisms of microcephaly. *Front Cell Neurosci* 14:115. <https://doi.org/10.3389/fncel.2020.00115>
16. Grinberg I, Northrup H, Ardinger H, Prasad C, Dobyns WB, Millen KJ (2004) Heterozygous deletion of the linked genes ZIC1 and ZIC4 is involved in Dandy-Walker malformation. *Nat Genet* 36:1053–1055. <https://doi.org/10.1038/ng1420>
17. Guidi S, Ciani E, Bonasoni P, Santini D, Bartesaghi R (2011) Widespread proliferation impairment and hypocellularity in the cerebellum of fetuses with down syndrome. *Brain Pathol* 21:361–373. <https://doi.org/10.1111/j.1750-3639.2010.00459.x>
18. Haldipur P, Aldinger KA, Bernardo S, Deng M, Timms AE, Overman LM et al (2019) Spatiotemporal expansion of primary progenitor zones in the developing human cerebellum. *Science* 366:454–460. <https://doi.org/10.1126/science.aax7526>
19. Haldipur P, Bharti U, Govindan S, Sarkar C, Iyengar S, Gressens P et al (2012) Expression of Sonic hedgehog during cell proliferation in the human cerebellum. *Stem Cells Dev* 21:1059–1068. <https://doi.org/10.1089/scd.2011.0206>
20. Haldipur P, Dang D, Aldinger KA, Janson OK, Guimiot F, Adle-Biasette H et al (2017) Phenotypic outcomes in Mouse and Human Foxc1 dependent Dandy-Walker cerebellar malformation suggest shared mechanisms. *Elife*. <https://doi.org/10.7554/eLife.20898>
21. Haldipur P, Gillies GS, Janson OK, Chizhikov VV, Mithal DS, Miller RJ et al (2014) Foxc1 dependent mesenchymal signalling drives embryonic cerebellar growth. *Elife*. <https://doi.org/10.7554/eLife.03962>
22. Kapur RP, Mahony BS, Finch L, Siebert JR (2009) Normal and abnormal anatomy of the cerebellar vermis in midgestational human fetuses. *Birth Defects Res A Clin Mol Teratol* 85:700–709. <https://doi.org/10.1002/bdra.20589>
23. Leto K, Arancillo M, Becker EB, Buffo A, Chiang C, Ding B et al (2016) Consensus paper: cerebellar development. *Cerebellum* 15:789–828. <https://doi.org/10.1007/s12311-015-0724-2>
24. Liao Y, Smyth GK, Shi W (2014) featureCounts: an efficient general purpose program for assigning sequence reads to genomic features. *Bioinformatics* 30:923–930. <https://doi.org/10.1093/bioinformatics/btt656>
25. Limperopoulos C, Soul JS, Gauvreau K, Huppi PS, Warfield SK, Bassan H et al (2005) Late gestation cerebellar growth is rapid and impeded by premature birth. *Pediatrics* 115:688–695. <https://doi.org/10.1542/peds.2004-1169>
26. Love MI, Huber W, Anders S (2014) Moderated estimation of fold change and dispersion for RNA-seq data with DESeq2. *Genome Biol* 15:550. <https://doi.org/10.1186/s13059-014-0550-8>
27. Phillips JJ, Mahony BS, Siebert JR, Lalani T, Fligner CL, Kapur RP (2006) Dandy-Walker malformation complex: correlation between ultrasonographic diagnosis and postmortem neuropathology. *Obstet Gynecol* 107:685–693. <https://doi.org/10.1097/01.AOG.0000200594.85483.8a>
28. Poretti A, Boltshauser E, Huisman T (2016) Pre- and postnatal neuroimaging of congenital cerebellar abnormalities. *Cerebellum* 15:5–9. <https://doi.org/10.1007/s12311-015-0699-z>
29. Rakic P, Sidman RL (1970) Histogenesis of cortical layers in human cerebellum, particularly the lamina dissecans. *J Comp Neurol* 139:473–500. <https://doi.org/10.1002/cne.901390407>
30. Russo R, Fallet-Bianco C (2007) Isolated posterior cerebellar vermal defect: a morphological study of midsagittal cerebellar vermis in 4 fetuses—early stage of Dandy-Walker continuum or new vermal dysgenesis? *J Child Neurol* 22:492–500. <https://doi.org/10.1177/0883073807299862>
31. Schlatterer SD, Sanapo L, du Plessis AJ, Whitehead MT, Mulkey SB (2021) The role of fetal MRI for suspected anomalies of the posterior Fossa. *Pediatr Neurol* 117:10–18. <https://doi.org/10.1016/j.pediatrneurol.2021.01.002>
32. Taggart JK, Walker AE (1942) Congenital Atresia of the foramina of Luschka and Magendie. *Arch Neuropsych* 48:583–612. <https://doi.org/10.1001/archneurpsyc.1942.02290100083008>
33. Vera Alvarez R, Pongor LS, Marino-Ramirez L, Landsman D (2019) TPMCalculator: one-step software to quantify mRNA abundance of genomic features. *Bioinformatics* 35:1960–1962. <https://doi.org/10.1093/bioinformatics/bty896>
34. Volpe JJ (2009) Cerebellum of the premature infant: rapidly developing, vulnerable, clinically important. *J Child Neurol* 24:1085–1104. <https://doi.org/10.1177/0883073809338067>
35. Volpe P, Contro E, De Musso F, Ghi T, Farina A, Tempesta A et al (2012) Brainstem-vermis and brainstem-tentorium angles allow accurate categorization of fetal upward rotation of cerebellar vermis. *Ultrasound Obstet Gynecol* 39:632–635. <https://doi.org/10.1002/uog.11101>

**Publisher's Note** Springer Nature remains neutral with regard to jurisdictional claims in published maps and institutional affiliations.

## Authors and Affiliations

Parthiv Haldipur<sup>1</sup>  · Silvia Bernardo<sup>2</sup> · Kimberly A. Aldinger<sup>1,3</sup> · Tarika Sivakumar<sup>1</sup> · Jake Millman<sup>1</sup> · Alexandria H. Sjoboen<sup>1</sup> · Derek Dang<sup>1</sup> · Danilo Dubocanin<sup>1</sup> · Mei Deng<sup>4</sup> · Andrew E. Timms<sup>5</sup> · Brian D. Davis<sup>6</sup> · Jasmine T. Plummer<sup>6</sup> · Kshitij Mankad<sup>7</sup> · Ozgur Oztekin<sup>8</sup> · Lucia Manganaro<sup>9</sup> · Fabien Guimiot<sup>10</sup> · Homa Adle-Biassette<sup>11,12</sup> · Rosa Russo<sup>13</sup> · Joseph R. Siebert<sup>14</sup> · Debora Kidron<sup>15</sup> · Giulia Petrilli<sup>16</sup> · Nathalie Roux<sup>16</sup> · Ferechte Razavi<sup>16</sup> · Ian A. Glass<sup>1,3,4</sup> · Cira Di Gioia<sup>9</sup> · Evelina Silvestri<sup>17</sup> · Kathleen J. Millen<sup>1,3,4</sup>

<sup>1</sup> Center for Integrative Brain Research, Seattle Children's Research Institute, Seattle, USA

<sup>2</sup> Department of Experimental Medicine, Sapienza University of Rome, Rome, Italy

<sup>3</sup> Brotman Baty Institute for Precision Medicine, Seattle, USA

<sup>4</sup> Department of Pediatrics, University of Washington, Seattle, USA

<sup>5</sup> Center for Developmental Biology and Regenerative Medicine, Seattle Children's Research Institute, Seattle, USA

<sup>6</sup> Center for Bioinformatics and Functional Genomics, Department of Biomedical Science, Cedars-Sinai Medical Center, Los Angeles, USA

<sup>7</sup> Department of Radiology, Great Ormond Street Hospital NHS Foundation Trust, London, UK

<sup>8</sup> Department of Neuroradiology, İzmir Bakırçay University, İzmir, Turkey

<sup>9</sup> Department of Radiological, Oncological and Pathological Sciences, Sapienza University of Rome, Rome, Italy

<sup>10</sup> Hôpital Robert-Debré, INSERM UMR 1141, Paris, France

<sup>11</sup> Department of Pathology, Hôpital Lariboisière, APHP, Paris, France

<sup>12</sup> UMR1141, Université Paris Diderot, Sorbonne Paris Cité, Paris, France

<sup>13</sup> Department of Pathology, University Medical Hospital, Salerno, Italy

<sup>14</sup> Department of Laboratories, Seattle Children's Hospital and Department of Pathology, University of Washington, Seattle, USA

<sup>15</sup> Department of Pathology, Meir Medical Center, Kfar Saba and Sackler School of Medicine, Tel Aviv University, Aviv-Yafo, Israel

<sup>16</sup> Hôpital Necker-Enfants Malades, APHP, Paris, France

<sup>17</sup> Perinatal Pathology Unit, Surgical Pathology Department, Azienda Ospedaliera San Camillo-Forlanini, Rome, Italy